Nanoscale

Ligand Exchange on Au38(SR)24: Substituent Site Effects of Aromatic Thiols

Journal:	*Nanoscale*
Manuscript ID	NR-ART-02-2020-001430.R1
Article Type:	Paper
Date Submitted by the Author:	19-Mar-2020
Complete List of Authors:	Li, Yingwei; Carnegie Mellon University, Chemistry Juarez-Mosqueda, Rosalba ; Univ of Pittsburgh Song, Yongbo; Anhui University, Zhang, Yuzhuo ; Carnegie Mellon University Chai, Jinsong; Anhui University Mpourmpakis, Giannis; University of Pittsburgh, Chemical and Petroleum Engineering Jin, Rongchao; Carnegie Mellon University, Chemistry

ARTICLE

Ligand Exchange on $Au_{38}(SR)_{24}$: Substituent Site Effects of Aromatic Thiols

Received 00th January 20xx,
Accepted 00th January 20xx

DOI: 10.1039/x0xx00000x

Yingwei Li[a], Rosalba Juarez-Mosqueda[b], Yongbo Song[c], Yuzhuo Zhang[a], Jinsong Chai[a], Giannis Mpourmpakis*[b], and Rongchao Jin*[a]

Understanding the critical roles of ligands (e.g. thiolate, SR) in forming metal nanoclusters of specific sizes has long been an intriguing task since the report of ligand-exchange-induced transformation of $Au_{38}(SR)_{24}$ to $Au_{36}(SR')_{24}$. Herein, we conduct a systematic study of ligand exchange on $Au_{38}(SC_2H_4Ph)_{24}$ with 21 incoming thiols and reveal that the size/structure preference is dependent on the substituent site. Specifically, *ortho*-substituted benzenethiols preserve the structure of $Au_{38}(SR)_{24}$, while *para*- or non-substituted benzenethiols cause the transformation to $Au_{36}(SR)_{24}$. Strong electron donating or withdrawing groups do not make a difference, but will inhibit full ligand exchange. Moreover, the crystal structure of $Au_{38}(SR)_{24}$ (SR = 2,4-methylbenzenthiolate) exhibits distinctive π···π stacking as well as "anagostic" interaction (indicated by substantially short Au···H distances). Theoretical calculations find the raised energies of frontier orbitals for aromatic ligand-protected Au_{38}, indicating decreased electronic stability. However, this adverse effect could be compensated by the Au···H-C interactions which improve the geometric stability when *ortho*-substituted benzenethiols are used. Overall, this work reveals the substituenet site effect based on the Au_{38} model, and stresses the long-neglected "anagostic" interactions on the surface of Au-SR NCs which improves the structural stability.

1 Introduction

Ligand-protected metal nanoclusters (NCs) of atomic precision have been appealing to researchers not only for their unusual properties due to quantum confinement and structural diversity, but for the opportunity to correlate the structures with the properties as well.[1,2] Thiols (HSR) are the most widely used ligands in producing Au NCs owing to strong Au-S bond. In the early works by the Tsukuda group,[3–5] a series of glutathione-protected $Au_n(SR)_m$ were separated and identified with mass spectroscopy (MS). To solve the total structures *via* single crystal X-ray diffraction, organic ligands were devised to achieve crystallization; for example, the structures of $Au_{25}(SR)_{18}$ and $Au_{38}(SR)_{24}$ were successfully attained with the help of 2-phenylethanethiol (PET),[6–8] and cyclohexanethiol was used to crystallize $Au_{18}(SR)_{14}$.[9,10] It was later found that 4-*tert*-butylbenzenthiol (TBBT, same abbrev. for the thiolate form) could give rise to a series of Au-SR NCs with face-centered cubic kernels,[11] while *tert*-butyl thiol was used to synthesize Au_{23}, Au_{30}, Au_{46} and Au_{65}.[12] For alloy NCs, the $[Au_{12+n}Cu_{32}(SR)_{30+n}]^{4-}$ series (n = 0, 2, 4, and 6) was prepared by 4-(trifluoromethyl) thiophenol;[13] whereas adamantanethiol produced a series of Au/Ag alloy clusters of structural differentiation *via* asymmetric Ag doping.[14]

In addition, the bulkiness of ligands was found to control the size of Au-SR NCs,[15] and the position of substituents on benzenethiolate ligands is also decisive as $Au_{130}(SR)_{50}$, $Au_{104}(SR)_{41}$, and $Au_{40}(SR)_{24}$ NCs were achieved by isomeric *para*-, *meta*-, and *ortho*-methylbenzenthiols, respectively.[16] The Ag_{16} and Ag_{32} NCs were prepared by 3,4-difluorothiophenol and 4-(trifluoromethyl) thiophenol, respectively,[17] whereas 2,4- and 2,5-dimethylbenzenethiols resulted in Ag_{40} and Ag_{46}, respectively.[18] Such size/structure selectivity dictated by different ligands are also demonstrated by ligand exchange,[19–23] implying that specific thiol would have its preference for certain magic sized metal-SR NCs over others.

The ligand effect on Au NCs was also studied theoretically.[24–26] Based on the early models derived from $[Au_{25}(SR)_{18}]^-$, $Au_{38}(SR)_{24}$, and $Au_{102}(SR)_{44}$, it was reported that the aliphatic thiolate-stabilized NCs have higher electrochemical and thermodynamic stability than the aromatic thiolate-stabilized counterparts.[24] Density function theory (DFT) analyses provided insights into the isomer stability of $Au_{24}(SR)_{20}$ and $Au_{28}(SR)_{20}$.[26–28]

The geometric/electronic structures of Au_{38} NCs and their properties have been studied for years.[29–32] Motivated by the importance of ligands in associating specific sizes by their stability, herein we conduct a systematic ligand exchange study on the $Au_{38}(PET)_{24}$ with 21 thiols, and illustrate how the substituent sites on aromatic thiols affect the structural stability of Au_{38}. Additionally, the crystal structure of $Au_{38}(2,4DMBT)_{24}$ shows

[a] *Department of Chemistry, Carnegie Mellon University, Pittsburgh, Pennsylvania 15213, United States.*
[b] *Department of Chemical Engineering, University of Pittsburgh, Pittsburgh, Pennsylvania 15261, United States.*
[c] *Department of Chemistry and Centre for Atomic Engineering of Advanced Materials, Anhui Province Key Laboratory of Chemistry for Inorganic/Organic Hybrid Functionalized Materials, Anhui University, Hefei, Anhui 230601, People's Republic of China.*

Electronic Supplementary Information (ESI) available: [details of any supplementary information available should be included here]. See DOI: 10.1039/x0xx00000x

significant $\pi\cdots\pi$ interactions between phenyl rings, and more importantly, "anagostic" interactions (i.e., Au···H-C) are also identified. Time-dependent DFT (TDDFT) calculations show an overall rise in energy for the electronic states of aromatic ligand-protected Au_{38}, indicating a reduced electronic stability; however, this disadvantage can be offset by the "anagostic" interactions. This work demonstrates the role of *ortho*-substituent on SPh in retaining the structure of Au_{38} by forming additional Au···H-C interactions.

2 Results and discussion

The synthesis of $Au_{38}(PET)_{24}$ is based on the literature.[7] As for the ligand exchange, 1 mg of pure $Au_{38}(PET)_{24}$ was dissolved in 1 mL of toluene and then mixed with ~1 mg or ~1 µL different incoming ligands (Scheme 1). The reactions were conducted at different temperatures (see discussions below). The product was washed repeatedly by methanol, and extracted by dichloromethane. In the following discussions, the acronyms for ligands (the same for the thiol and thiolate forms) are as defined in Scheme 1.

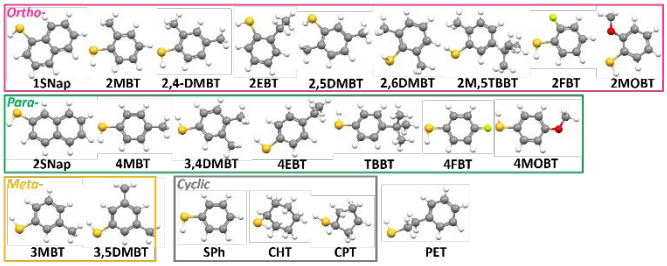

Scheme 1 The thiols used in ligand exchange with $Au_{38}(PET)_{24}$. Color codes: yellow = S; grey = C; white = H; red = O; and light green = F.

2.1 Ligand exchange by benzenethiol with *ortho*-substituent

We first discuss the ligand exchange with *ortho*-substituted benzenethiols. Time-dependent UV-vis absorption spectra and corresponding MALDI MS spectra (Figure S1) show that 2-methylbenzenthiol (2MBT) or 1-naphthalenethiol (1SNap) cannot completely replace PET on $Au_{38}(SR)_{24}$ at room temperature. However, at 80 °C, pure $Au_{38}(2MBT)_{24}$ and $Au_{38}(1SNap)_{24}$ were obtained. It should be noted that the highest peak in MS spectra corresponds to $Au_{38}(PET)_{24}$, while for conjugated-thiolate-protected Au_{38}, one ligand is detached from the clusters, and the fragment by losing $Au_4(SR)_4$ becomes more prominent (Figure S1C/F).

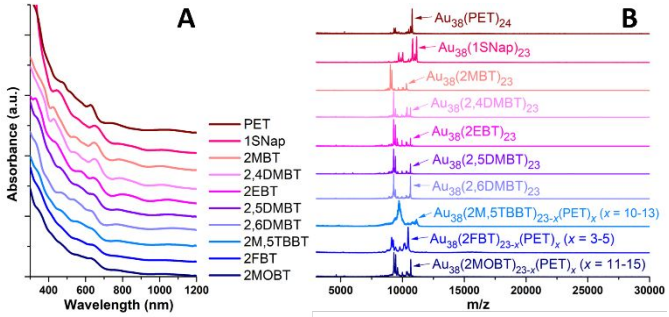

Figure 1 (A) UV-vis spectra of different $Au_{38}(SR)_{24}$ NCs by ligand exchange on $Au_{38}(PET)_{24}$ with HSPh-X (X takes at least one *ortho*-position) at 45 °C, and (B) corresponding MALDI-MS spectra.

The experiments were then set at 45 °C for ligand exchange with more types of *ortho*-substituted benzenethiols (Figure S2). It is found that moderate heating is enough for full exchange with 1SNap, 2MBT, 2,4-dimethylbenzenethiol (2,4DMBT), 2-ethylbenzenethiol (2EBT), 2,5-dimethylbenzenethiol (2,5DMBT), and 2,6-dimethylbenzenethiol (2,6DMBT) according to MALDI-MS spectra (Figure 1). However, the trials with 2-methyl-5-*tert*-butylbenzenthiol (2M,5TBBT), 2-fluorobenzenethiol (2FBT) or 2-methoxybenzenethiol (2MOBT) were not complete, evidenced by the formation of $Au_{38}(SR)_{23-x}(PET)_x$; we even repeated the three experiments at 80 °C (Figure S3), in which the number of exchanged ligands was increased, but some impurities were introduced as well.

Therefore, it is clear that as long as the incoming thiol has an *ortho*-substituted group on the phenyl ring, $Au_{38}(SR)_{24}$ is always favored. But when a bulky group (e.g. ^{t}Bu group), strong electron donating (-OCH_3) or withdrawing (-F) group is involved, the ligand exchange will be disturbed.

2.2 Ligand exchange by benzenethiol with *meta*-/*para*-substituent

Based on the results from *ortho*-substituted benzenethiols, we then conducted the ligand exchange with *para*- or *meta*-substituted benzenethiols**,** including 2-naphthalenethiol (2SNap), 4-methylbenzenethiol (4MBT), 3,4-dimethylbenzenethiol (3,4DMBT), 4-ethylbenzenethiol (4EBT), 4-*tert*-butyl-benzenethiol (TBBT), 4-fluorobenzenethiol (4FBT), 4-methoxybenzenethiol (4MOBT), 3-methylbenzenethiol (3MBT) and 3,5-dimethylbenzenethiol (3,5DMBT), at room temperature (RT) (Figure S4). Although ligand exchange was incomplete at RT, $Au_{38}(SR)_{24}$ NCs protected by mixed thiols were the only products (Figure 2); whereas higher temperatures would introduce structural transformation (*vide infra*). On a note, because 3,4DMBT and 4EBT have the same molecular weight as that of PET, the numbers of incoming ligands cannot be determined by MS, but should be similar to the cases of 2SNap or 4MBT. The $Au_{38}(TBBT)_{23-x}(PET)_x$ NCs show identical characteristics to the intermediate formed during the preparation of $Au_{36}(TBBT)_{24}$ in previous work.[21]

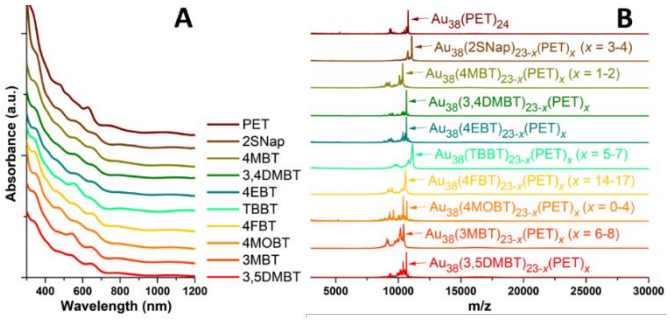

Figure 2 (A) UV-vis spectra of different $Au_{38}(SR)_{24}$ NCs by ligand exchange on $Au_{38}(PET)_{24}$ with HSPh-X (X takes the *meta*-, and/or *para*- position(s)) at RT, and (B) corresponding MALDI-MS spectra.

The absorption peak at the longest wavelength corresponds to the HOMO-LUMO gap for *para*- and *meta*-substituted benzenthiolate-protected Au_{38} and is observed to red-shift in all cases (Figure S5), indicating that the gap becomes smaller. It is

worth noting that our results are different from the theoretical results that the *para*-substituents in $[Au_{25}(SPhX)_{18}]^-$ (X = H, F, Cl, Br, CH_3, and OCH_3) moderately shift the HOMO/LUMO energy states but without affecting the gap.[33]

2.3 Ligand exchange by cyclic thiols with no substituent

Finally, we investigate cyclic-ligands such as non-conjugated cyclohexanethiol (CHT) and cyclopentanethiol (CPT), as well as conjugated benzenethiol (HSPh). The ligand-exchange processes were also monitored at RT (Figure S6), and the resultant $Au_{38}(SPh)_{24}$ NCs were almost the same as reported previously,[34] except one or two PET ligands left in the final product (Figure 3).

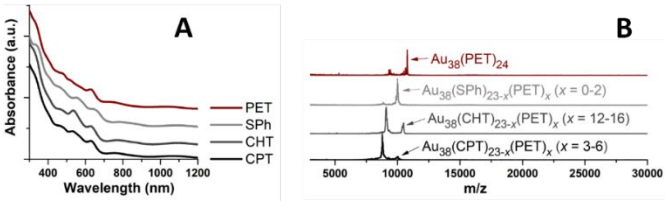

Figure 3 (A) UV-vis spectra of different $Au_{38}(SR)_{24}$ NCs by ligand exchange on $Au_{38}(PET)_{24}$ with cyclic ligands at RT, and (B) the corresponding MALDI-MS spectra.

It has been demonstrated that TBBT, CPT and SPh result in $Au_{36}(SR)_{24}$ at 80 °C.[21,34,35] Therefore, we repeated the ligand exchange with HSPh-X (X takes *meta*-, and/or *para*- site(s)) as well as cyclic ligands at 80 °C (Figure S7). Except the *meta*-substituted benzenethiol and CHT, all other ligands gave $Au_{36}(SR)_{24}$ as the product due to ligand-exchange-induced transformation. Only the 4FBT and 4MOBT trials gave slightly incomplete ligand exchange (Figure S8).

Thus, it is also clear that, although $Au_{38}(SR)_{24-x}(PET)_x$ retain the original structure at RT with partial ligand replacement, *meta*-substituted thiols cannot stabilize Au_{38} at 80 °C (decomposed); whereas *para*- or non-substituted benzenethiol drives the transformation from Au_{38} to Au_{36} as long as the thermodynamic barrier can be overcome. The case of 2,4DMBT was further tested at 80 °C as it has both *ortho*- and *para*-substituents, and pure $Au_{38}(2,4DMBT)_{24}$ was produced (Figure S9), indicating *ortho*-substituent is more influential than other sites.

2.4 $Au_{38}(2,4DMBT)_{24}$ *vs.* $Au_{38}(PET)_{24}$ structures

In our attempts to crystalize all the $Au_{38}(SR)_{24}$ NCs, only $Au_{38}(2MBT)_{24}$ and $Au_{38}(2,4DMBT)_{24}$ NCs were able to form single crystals (*via* diffusing methanol into dichloromethane solution over 2 days), but the crystal quality of $Au_{38}(2MBT)_{24}$ was not sufficient. The crystal structure of $Au_{38}(2,4DMBT)_{24}$ was successfully determined by X-ray crystallography.[36]

Similar to the crystal structure of the starting $Au_{38}(PET)_{24}$, $Au_{38}(2,4DMBT)_{24}$ also has a bi-icosahedral Au_{23} kernel which is protected by three $Au(SR)_2$ motifs at the waist and six $Au_2(SR)_3$ motifs resembling two tri-blade fans at the top and bottom. However, the differences between the two NCs are obvious. The two tri-blade fans in $Au_{38}(PET)_{24}$ are arranged in a staggered conformation by ~60° to each other (Figure 4A); while for $Au_{38}(2,4DMBT)_{24}$, one fan rotates only by ~45° relative to the other along the C_3 axis (Figure 4B). Besides, each $Au(SR)_2$ motif is parallel to the two adjacent $Au_2(SR)_3$ motifs in $Au_{38}(2,4DMBT)_{24}$ but it is not so in $Au_{38}(PET)_{24}$ (Figure 4A/B, indicated by blue lines). In addition, the $Au_{38}(PET)_{24}$ is of C_1 symmetry and the NCs form a triclinic unit cell, whereas $Au_{38}(2,4DMBT)_{24}$ is of D_3 symmetry and the NCs are packed into a trigonal unit cell (Figure 4C/D). This observation is consistent with our earlier one that the symmetry of NCs and the symmetry of the unit cell are highly correlated.[14]

The changes in the arrangement of staple motifs and the symmetry of the NCs and unit cell are caused by the introduced new ligand. Significant $\pi\cdots\pi$ interactions in solid state are observed between the 2,4DMBT ligands, i.e. the phenyl rings of adjacent $Au_2(SR)_3$ motifs in the same tri-blade fan (Figure 4E, three pairwise interactions marked in different greens, total six pairs), and those in different tri-blade fans (Figure 4F, three pairwise interactions marked in different pinks). Such interactions on the surface of $Au_{38}(2,4DMBT)_{24}$ restrict the freedom of these motifs and improve the symmetry of the cluster. This can also be understood from the experimental perspective that heating (at least 45°C, Figure 1) is required for full ligand-exchange with *ortho*-substituted benzenethiols as there is a thermodynamic barrier.

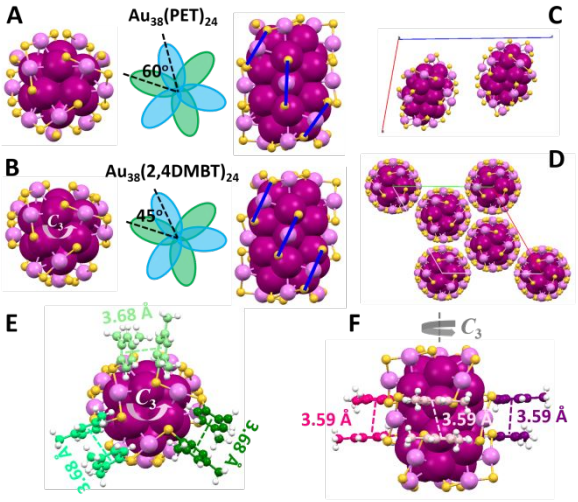

Figure 4 Top/front view, and the schematic diagram of two overlapped tri-blade fans of (A) $Au_{38}(PET)_{24}$ and (B) $Au_{38}(2,4DMBT)_{24}$. (C) The triclinic unit cell of $Au_{38}(PET)_{24}$; (D) the trigonal unit cell of $Au_{38}(2,4DMBT)_{24}$. The $\pi\cdots\pi$ interactions (E) in the same tri-blade fan, and (F) in different tri-blade fans of $Au_{38}(2,4DMBT)_{24}$.

Despite that the strong $\pi\cdots\pi$ interactions could explain the high stability of $Au_{38}(2,4DMBT)_{24}$, one should realize that solvation in solution phase might destroy $\pi\cdots\pi$ interactions. As we discussed in Sections 2.1-2.3, *ortho*-substituted benzenethiols act differently in stabilizing $Au_{38}(SR)_{24}$ compared to other thiols, hence, there should be certain other interaction that is exclusive to the *ortho*-substituted SPh-X ligands. This leads us to look into the possible Au···H-C interactions on the surface. As shown in Figure 5, such interactions are indeed found in $Au_{38}(2,4DMBT)_{24}$, as the *ortho*-substituent's H atoms show substantially shorter distances to nearby Au atoms, including intra-motif interactions (marked by green in Figure 5A/B) and inter-motif interactions (blue in Figure

5A). All these interactions, with *d*(Au···H) of 2.54-2.82Å, and ∠Au-H-C of 119.7-155.0°.

"Agostic" interactions of the type M···H-C were observed in many organometallic compounds with the M atoms from the early transition metals;[37,38] whereas the term "anagostic" was proposed to describe the M···H-C interactions for late transition elements.[39] The difference between "agostic" and "anagosic" interactions is based on M···H distances as well as M-H-C angles, and for the latter, *d*(M···H)=2.3-2.9Å, and ∠M-H-C=110-170°.[38] Such interactions were previously discussed in gold(I) complexes,[40–42] but rarely in Au NCs due to the typical geometry being unfavorable for such interactions. Konishi et al. recently reported substantially short Au···H distances (*d*(M···H) ≈ 2.60-2.87 Å) in $[Au_6]^{2+}$, indicating attractive interactions critical to affect the stability of the cluster.[36] The observed *d*(Au···H) of 2.54-2.82Å, and ∠Au-H-C of 119.7-155.0° in $Au_{38}(2,4DMBT)_{24}$ are within the region of "anagostic" definition, and moreover, since the $Au_{38}(2,4DMBT)_{24}$ NC is of D_3 symmetry, such "anagostic" interactions from the $Au_2(SR)_3$ motifs are 6 times in total for the whole $Au_{38}(2,4DMBT)_{24}$ NC, and the interactions from the $Au(SR)_2$ motifs (Figure 5B) also triple, i.e., multiple "anagostic" interactions on the surface of a single nanocluster.

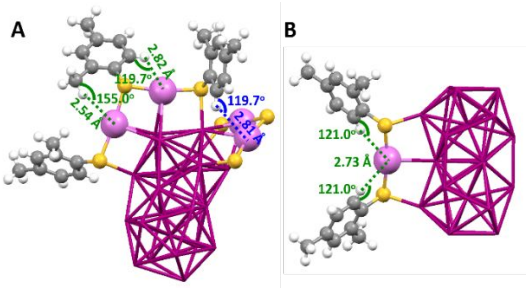

Figure 5 The "anagostic" interactions between Au and H from (A) dimeric $Au_2(2,4DMBT)_3$ motif ligands; (B) the monomeric $Au(2,4DMBT)_2$ motif ligands.

By contrast, in the previously reported $Au_{38}(PET)_{24}$ structure, the shortest *d*(Au···H) was 2.96-3.26Å and the corresponding ∠Au-H-C angles were 79.4-118.7°, which cannot be assigned as "anagostic" interactions (Figure S10). In other words, the average *d*(Au···H) in $Au_{38}(2,4DMBT)_{24}$ is significantly shortened by ~14% compared to that in $Au_{38}(PET)_{24}$, indicating much stronger surface Au···H interactions which contribute to the stability of the NC.[36] Thus, the *ortho*-substituents on benzenethiolates are critical to form the effective "anagostic" interactions.

Accordingly, the Au_{staple}-Au_{kernel} bond lengths of $Au_{38}(2,4DMBT)_{24}$ NCs are affected by "anagostic" interactions as well, and the average bond length of 3.04 Å is 2.3% shorter than that of $Au_{38}(PET)_{24}$ (3.11 Å), indicating higher geometric stability for $Au_{38}(2,4DMBT)_{24}$.

2.5 $Au_{38}(2,4DMBT)_{24}$ *vs.* $Au_{38}(PET)_{24}$ TDDFT comparison

Based on the total structures of the two $Au_{38}(SR)_{24}$ NCs, we are able to gain more insights into their electronic structures. In our TDDFT, we retain the crystal symmetries of the NCs and the full ligands are incorporated into the calculations (Figure S11). The local projected density of states (LPDOS) per atom are given in Figure S12. For both $Au_{38}(SR)_{24}$ NCs, the density of states are mainly delocalized over the $Au_{38}S_{24}$ frame. However, it is clear that in the case of $Au_{38}(2,4DMBT)_{24}$, the local *p* states of C atoms significantly contribute to the frontier molecular orbitals (*i.e.* HOMO-4 to LUMO+4), while for $Au_{38}(PET)_{24}$, the carbon contribution is almost neglectable (Figure S12).

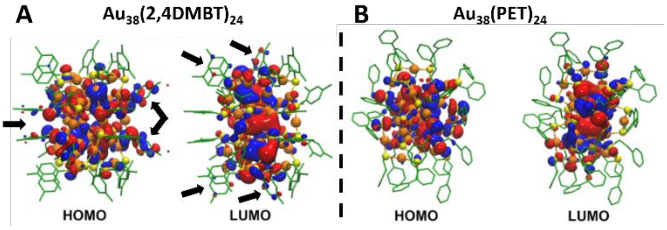

Figure 6. Kohn-Sham diagrams of HOMO and LUMO for (A) $Au_{38}(2,4DMBT)_{24}$ and (B) $Au_{38}(PET)_{24}$ NCs.

The Kohn–Sham (KS) diagrams of HOMO and LUMO for the two Au_{38} NCs are shown in Figure 6, and more frontier orbitals can be found in Figure S13. The diagrams of $Au_{38}(2,4DMBT)_{24}$ (Figure 6A, Figure S13A) are well consistent with the reports by Aikens and co-workers on $Au_{38}(SH)_{24}$ and $Au_{38}(SCH_3)_{24}$ of D_3 symmetry.[43,44] As for the frontier orbitals near the HOMO-LUMO gap of $Au_{38}(PET)_{24}$, the orbital symmetry is less well-defined (Figure 6B, Figure S13B) compared to those of $Au_{38}(2,4DMBT)_{24}$ in which Σ, Π and Δ characters can be clearly identified (Figure 6A, Figure S13A). More importantly, for HOMO-2 to LUMO+2 orbitals, it is visualized that the electron density is even delocalized from the $Au_{38}S_{24}$ frame to the aromatic rings of 2,4DMBT (Figure 6A black arrows, Figure S13A), while no electron density can be found on the $-CH_2CH_2Ph$ groups (Figure 6B, Figure S13B).

It was reported that for Au NCs protected by terminal alkynyls, as Au kernel and R groups could be coupled *via* C≡C, the frontier MOs and optical properties would be affected in a more profound way than in Au-SR NCs.[45] In alkynyl-protected Au_{25}, C(*p*) character of alkyne ligands is found to be mainly involved in high-energy transitions, but only slightly affect the HOMO-LUMO transition.[46] In contrast, the $\pi\cdots\pi$ stacking of phenyl rings in $Au_{38}(2,4DMBT)_{24}$ solid state leads to meaningful differences in the electronic structure, especially the HOMO and LUMO as well as adjacent orbitals.

The simulated optical spectra of both $Au_{38}(SR)_{24}$ NCs are shown in Figure S14A/B. Except the slightly blue-shifted peak **a** (HOMO/HOMO-1 to LUMO/LUMO+1 transitions), all other peaks **b/c/d** of $Au_{38}(2,4DMBT)_{24}$ are red-shifted by ~0.1-0.2 eV with respect to the corresponding peaks **a'/b'/c'/d'** of $Au_{38}(PET)_{24}$. The electronic transitions contributing to these main absorption peaks (**a/b/c/d** or **a'/b'/c'/d'**) are given in Table S1. In both NCs, the HOMO and HOMO-1 are nearly degenerated, whereas LUMO and LUMO+1 are closer for $Au_{38}(2,4DMBT)_{24}$ than $Au_{38}(PET)_{24}$ (Figure S14C, Table S2). This is reflected in experimental spectra by a slightly larger energy gap, i.e. blue-shifted peak **a** (Figure S14A). On the other hand, the energy difference between HOMO-1 and HOMO-2 increases from 0.162 eV in $Au_{38}(2,4DMBT)_{24}$ to 0.331 eV in $Au_{38}(PET)_{24}$. This explains the obvious shifts of peaks **b/c/d** to lower energies for $Au_{38}(2,4DMBT)_{24}$, and a shoulder in peak **b** (Figure S14A, blue arrow) due to peak splitting. The overall higher energy states for $Au_{38}(2,4DMBT)_{24}$ compared to $Au_{38}(PET)_{24}$ (Figure S14C, indicated by blue dashed arrows), especially the much higher

HOMO-2, suggesting less electronic stability although the two NCs have similar energy gaps.

The observation that $Au_{38}(PET)_{24}$ is more electronically stable in above theoretical analysis leads us to check the atomic charges of the two clusters (Table S3). The average atomic charges of metal atoms in $Au_{38}(PET)_{24}$ are slightly less positive (by 0.46 e per Au_{38}) than those in $Au_{38}(2,4DMBT)_{24}$. However, the S atoms in $Au_{38}(PET)_{24}$ hold much more negative charge (by -1.41 e more per S_{24}) than $Au_{38}(2,4DMBT)_{24}$. We attribute this greater electron withdrawing effect of S atoms in $Au_{38}(PET)_{24}$ to the enhanced stability of its molecular orbitals of HOMO-2 and below which hence results in the blue-shift of absorption peaks **b'/c'/d'** (Figure 7A/B), which is consistent to the calculations on Au_{38} before.[24]

The question is, if $Au_{38}(SPh\text{-}X)_{24}$ NCs (aromatic thiolate as the stabilizer) are less electronically stable than $Au_{38}(PET)_{24}$ (non-aromatic stabilizer), why can they sustain the harsh ligand-exchange condition of 80 °C? We rationalize that the $\pi\cdots\pi$ interactions in the solid state, and more importantly, the distinctive "anagostic" Au···H-C interactions on the surface (see Section 2.4) should largely improve the geometric stability and effectively offset the loss in electronic stability.

2.6 Summary on the ligand exchange of $Au_{38}(PET)_{24}$

A summary on the ligand exchange of $Au_{38}(PET)_{24}$ is given in Table 1. Complete ligand exchange with *ortho*-substituted SPh-X cannot be done on Au_{38} at RT, but requires higher temperatures; ligand exchange with other ligands without an *ortho*-substitution cannot be completed on Au_{38} at RT except for SPh (almost complete), while at high temperatures, structural transformation to Au_{36} is inevitable, if not decomposed.

Table 1 Summary of ligand exchange on $Au_{38}(PET)_{24}$ at different temperatures, and the lowest-energy absorption peak positions of the ligand-exchanged Au_{38} (tested at 295K and 80K).

		RT	45 °C	80 °C	Au_{38} 295K (eV)	Au_{38} 80K (eV)
ref	PET				1.22	1.19
Ortho-	1SNap	→	√	√	1.25	1.22
	2MBT	→	√	√	1.29	1.23
	2,4DMBT	/	√	√	1.28	1.22
	2EBT	/	√	/	1.28	1.18
	2,5DMBT	/	√	/	1.22	1.18
	2,6DMBT	/	√	/	1.19	1.15
	2M,5TBBT	/	→	→	1.19	/
	2FBT	/	→	→	1.24	1.20
	2MOBT	/	→	→	1.24	1.20
Para-	2SNap	→	/	Δ	1.16	1.14
	4MBT	→	/	Δ	1.19	1.16
	3,4DMBT	→	/	Δ	1.16	1.12
	4EBT	→	/	Δ	1.15	1.15
	TBBT	→	/	Δ [21]	1.07	/
	4FBT	→	/	Δ	1.17	1.15
	4MOBT	→	/	Δ	1.16	1.14
Meta-	3MBT	→	/	×	1.12	/
	3,5MBT	→	/	×	1.14	/
Cyclic-	SPh	√	/	Δ	1.14	1.12
	CHT	→	/	×	1.16	1.12
	CPT	→	/	Δ [35]	1.18	1.13

→ ligand exchange incomplete; √ ligand exchange complete; Δ structural transformed; × decomposed; / not performed.

The cryogenic optical absorption spectra of $Au_{38}(SR)_{24}$ NCs after ligand exchange were measured at 80 K in 2-methyltetrahydrofuran (Figure 7). All the peaks become more prominent with blue-shifts compared to those at room temperature. The spectrum of $Au_{38}(PET)_{24}$ is well consistent to the literature.[47] Besides, the spectrum of $Au_{38}(SPh)_{24}$ at low temperature also agrees with the reported data.[34] Generally, after ligand exchange, peaks **b/c** of the resulted Au_{38} all shift to lower energy, especially those capped by aromatic ligands, and there is a unanimous splitting in peak **b** (marked in shadow, Figure 7). Such a peak splitting is consistent with the calculated split transitions (Figure S14C). We also note that for Au_{38} NCs protected by *ortho*-substituted SPh-X, the absorption peaks at the lowest energy (peak **a**) are generally blue-shifted comparing to the $Au_{38}(PET)_{24}$ reference, while for other Au_{38} NCs protected by ligands without *ortho*-substitution, the corresponding peaks **a** are all clearly red-shifted (Table 1, Figure 7). The conformance in optical properties related to the substituent sites implies that the *ortho*-substituents on benzenethiolate play a critical role in the stability of Au_{38} by forming additional "anagostic" interactions on the NC surface, while the *para*-substituents drive the structural transformation to Au_{36}.

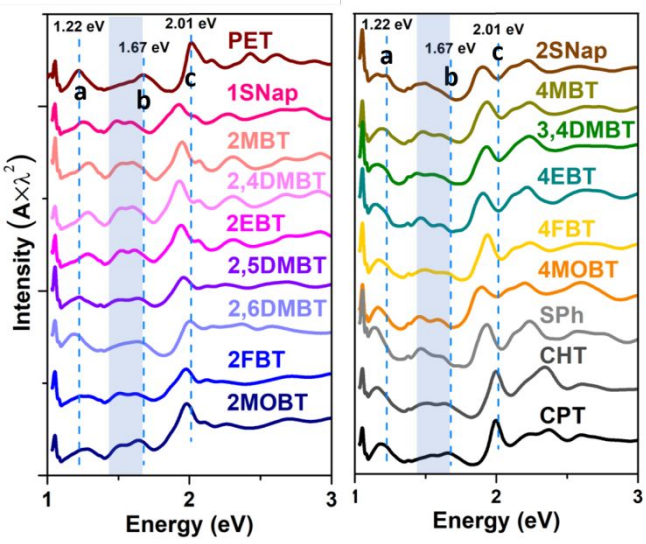

Figure 7 Cryogenic UV-vis-NIR spectra (80 K) of different $Au_{38}(SR)_{24}$ NCs. Dashed lines indicate the absorption peak positions of $Au_{38}(PET)_{24}$ at 80 K.

Conclusions

In summary, in order to understand the ligand preference for specific size Au-SR NCs, we have performed detailed ligand exchanges on $Au_{38}(PET)_{24}$ with as many as 21 different incoming thiols. It is clear that the *ortho*-substituted SPh-X retains the structure of $Au_{38}(SR)_{24}$, while the *para*- or non-substituted SPh(X) causes the transformation to $Au_{36}(SR)_{24}$. Strong electron-donating or -withdrawing groups do not make any difference, but hamper full ligand exchange. Our study on the crystal structure of $Au_{38}(2,4DMBT)_{24}$ identifies distinctive π···π interactions and more importantly, the "anagostic" interactions which are rare in nanoclusters, and interestingly,

both types of interactions are absent in the $Au_{38}(PET)_{24}$. TDDFT shows that for aromatic ligand-protected Au_{38}, the electron density extends from the Au-S frame to the ligands, and the peaks in the visible region red-shift due to the much-increased HOMO-2 energy, indicating decreased electronic stability. However, this destabilization is effectively compensated by the "anagostic" interactions observed in Au_{38} protected with the *ortho*-substituted SPh, which enhances the geometric stability of $Au_{38}(2,4DMBT)_{24}$.

Conflicts of interest

There are no conflicts to declare.

Acknowledgements

We acknowledge the financial support from the National Science Foundation (NSF DMR-1808675 and CBET-CAREER program under Grant No. 1652694). Computational support was provided by the Center for Research Computing (CRC) at the University of Pittsburgh as well as the Extreme Science and Engineering Discovery Environment (XSEDE), which is supported by the NSF (ACI-1548562).

Notes and references

1 R. Jin, C. Zeng, M. Zhou, Y. Chen, *Chem. Rev.*, 2016, **116**, 10346.
2 I. Chakraborty, T. Pradeep, *Chem. Rev.*, 2017, **117**, 8208.
3 Y. Negishi, Y. Takasugi, S. Sato, H. Yao, K. Kimura, T. Tsukuda, *J. Am. Chem. Soc.*, 2004, **126**, 6518.
4 Y. Negishi, K. Nobusada, T. Tsukuda, *J. Am. Chem. Soc.*, 2005, **127**, 5261.
5 H. Tsunoyama, T. Tsukuda, *J. Am. Chem. Soc.* 2009, **131**, 18216.
6 M. Zhu, C. M. Aikens, F. J. Hollander, G. C. Schatz, R. Jin, *J. Am. Chem. Soc.*, 2008, **130**, 5883.
7 H. Qian, Y. Zhu, R. Jin, *ACS NANO* 2009, **3**, 3795.
8 H. Qian, W. T. Eckenhoff, Y. Zhu, T. Pintauer, R. Jin, *J. Am. Chem. Soc.*, 2010, **132**, 8280.
9 S. Chen, S. Wang, J. Zhong, Y. Song, J. Zhang, H. Sheng, Y. Pei, M. Zhu, *Angew. Chem. Int. Ed.*, 2015, **54**, 3145.
10 A. Das, C. Liu, H. Y. Byun, K. Nobusada, S. Zhao, N. L. Rosi, R. Jin, *Angew. Chem. Int. Ed.*, 2015, **54**, 3140.
11 C. Zeng, Y. Chen, K. Iida, K. Nobusada, K. Kirschbaum, K. J. Lambright, R. Jin, *J. Am. Chem. Soc.*, 2016, **138**, 3950.
12 T. C. Jones, L. Sumner, G. Ramakrishna, M. bin Hatshan, A. Abuhagr, S. Chakraborty, A. Dass, *J. Phys. Chem. C* 2018, **122**, 17726.
13 H. Yang, Y. Wang, J. Yan, X. Chen, X. Zhang, H. Häkkinen, *J. Am. Chem. Soc.*, 2014, **136**, 7197.
14 Y. Li, T.-Y. Luo, M. Zhou, Y. Song, N. L. Rosi, R. Jin, *J. Am. Chem. Soc.*, 2018, **140**, 14235.
15 P. J. Krommenhoek, J. Wang, N. Hentz, A. C. Johnston-Peck, K. A. Kozek, G. Kalyuzhny, J. B. Tracy, *ACS NANO* 2012, **6**, 4903.
16 Y. Chen, C. Zeng, D. R. Kauffman, R. Jin, *Nano Lett.*, 2015, **15**, 3603.
17 H. Yang, Y. Wang, N. Zheng, *Nanoscale* 2013, **5**, 2674.
18 J. Chai, S. Yang, Y. Lv, T. Chen, S. Wang, H. Yu, M. Zhu, *J. Am. Chem. Soc.*, 2018, **140**, 15582.
19 T. Higaki, M. Zhou, K. J. Lambright, K. Kirschbaum, M. Y. Sfeir, R. Jin, *J. Am. Chem. Soc.* 2018, **140**, 5691.
20 C. Zeng, Y. Chen, K. Kirschbaum, K. Appavoo, M. Y. Sfeir, R. Jin, *Sci. Adv.*, 2015, **1**:e1500045.
21 C. Zeng, C. Liu, Y. Pei, R. Jin, *ACS NANO* 2013, **7**, 6138.
22 C. Zeng, T. Li, A. Das, N. L. Rosi, R. Jin, *J. Am. Chem. Soc.*, 2013, **135**, 10011.
23 Q. Shi, Z. Qin, C. Yu, S. Liu, H. Xu, G. Li, *Nanoscale* 2020, **12**, 4982.
24 J. Jung, S. Kang, Y.-K. Han, *Nanoscale* 2012, **4**, 4206.
25 J. Zhong, X. Tang, J. Tang, J. Su, Y. Pei, *J. Phys. Chem. C* 2015, **119**, 9205.
26 Y. Chen, C. Liu, Q. Tang, C. Zeng, T. Higaki, A. Das, D. -e. Jiang, N. L. Rosi, R. Jin, *J. Am. Chem. Soc.*, 2016, **138**, 1482.
27 Q. Tang, R. Ouyang, Z. Tian, D. -e. Jiang, *Nanoscale* 2015, **7**, 2225.
28 A. Das, T. Li, G. Li, K. Nobusada, C. Zeng, N. L. Rosi, R. Jin, *Nanoscale* 2014, **6**, 6458.
29 L. Cheng, C. Ren, X. Zhang, J. Yang, *Nanoscale* 2013, **5**, 1475.
30 X. Nie, C. Zeng, X. Ma, H. Qian, Q. Ge, H. Xu, R. Jin, *Nanoscale* 2013, **5**, 5912.
31 B. Molina, A. Sánchez-Castillo, S. Knoppe, I. L. Garzón, T. Bürgi, A. Tlahuice-Flores, *Nanoscale* 2013, **5**, 10956.
32 Y. Li, Y. Chen, S. D. House, S. Zhao, Z. Wahab, J. C. Yang, R. Jin, *ACS Appl. Mater. Interfaces* 2018, **10**, 29425.
33 C. M. Aikens, *J. Phys. Chem. Lett.* 2010, **1**, 2594.
34 M. Rambukwella, S. Burrage, M. Neubrander, O. Baseggio, E. Aprà, M. Stener, A. Fortunelli, A. Dass, *J. Phys. Chem. Lett.* 2017, **8**, 1530.
35 A. Das, C. Liu, C. Zeng, G. Li, T. Li, N. L. Rosi, R. Jin, *J. Phys. Chem. A* 2014, **118**, 8264.
36 S. Zhuang, L. Liao, J. Yuan, N. Xia, Y. Zhao, C. Wang, Z. Gan, N. Yan, L. He, J. Li, H. Deng, Z. Guan, J. Yang, Z. Wu, *Angew. Chem. Int. Ed.*, 2019, **58**, 4510.
37 M. A. Bakar, M. Sugiuchi, M. Iwasaki, Y. Shichibu, K. Konishi, *Nat. Commun.*, 2017, **8**:576.
38 M. Brookhart, M. L. H. Green, L.-L. Wong, *Prog. Inorg. Chem.*, **36**, 1.
39 M. Brookhart, M. L. H. Green, G. Parkin, *Proc. Natl. Acad. Sci.*, 2007, **104**, 6908.
40 W. I. Sundquist, D. P. Bancroft, S. J. Lippard, *J. Am. Chem. Soc.*, 1990, **112**, 1590.
41 H. Schmidbaur, H. G. Raubenheimer, L. Dobrzańska, *Chem. Soc. Rev.*, 2014, **43**, 345.
42 H. Schmidbaur, *Angew. Chem. Int. Ed.*, 2019, **58**, 5806.
43 M. Rigoulet, S. Massou, E. D. Sosa Carrizo, S. Mallet-Ladeira, A. Amgoune, K. Miqueu, D. Bourissou, *Proc. Natl. Acad. Sci.*, 2019, **116**, 46.
44 O. Lopez-Acevedo, H. Tsunoyama, T. Tsukuda, H. Häkkinen, C. M. Aikens, J. Am. Chem. Soc. 2010, **132**, 8210.
45 K. L. D. M. Weerawardene, E. B. Guidez, C. M. Aikens, *J. Phys. Chem. C* 2017, **121**, 15416.
46 N. Kobayashi, Y. Kamei, Y. Shichibu, K. Konishi, *J. Am. Chem. Soc.*, 2013, **135**, 16078–16081.
47 J.-J. Li, Z.-J. Guan, Z. Lei, F. Hu, Q.-M. Wang, *Angew. Chem. Int. Ed.*, 2019, **58**, 1083.
48 M. S. Devadas, S. Bairu, H. Qian, E. Sinn, R. Jin, G. Ramakrishna, *J. Phys. Chem. Lett.*, 2011, **2**, 2752.

TOC

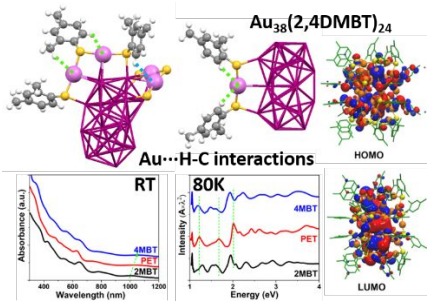

Ligand-exchange on $Au_{38}(SR)_{24}$ with 21 different thiols reveals the substituent-site effects of ligands on nanocluster transformation, and "anagostic" interactions are observed.